Low-Coherence Brillouin Optical Correlation-Domain Reflectometry Based on Periodic Pseudo-Random Modulation

Kenta Otsubo, Guangtao Zhu, Kohei Noda, *Member, IEEE*, Takaki Kiyozumi, *Student Member, IEEE*, Hiroshi Takahashi, Yusuke Koshikiya, and Yosuke Mizuno, *Senior Member, IEEE*

***Abstract*—Brillouin optical correlation-domain reflectometry (BOCDR) is a technique for measuring the distribution of strain and temperature along an optical fiber, offering advantages such as operation with light injection from one end of the sensing fiber, relatively high spatial resolution, and random-access capability to sensing points. However, it faces a trade-off between spatial resolution and measurement range. In response, low-coherence BOCDR using a randomly modulated light source has been proposed, but this method requires a variable delay line for scanning the measurement position, limiting the measurement range. This paper proposes low-coherence BOCDR based on periodic pseudo-random modulation to address this issue and demonstrates its proof-of-concept operation. First, the dependence of the light source output spectrum on modulation parameters is investigated using a delayed self-homodyne method, showing the potential to resolve the trade-off between spatial resolution and measurement range. Subsequently, we demonstrate the capability of measuring strain distribution along optical fibers without a variable delay line under multiple conditions. Further, we show through simulation that this method can perform more accurate distributed strain measurements than standard BOCDR.**

***Index Terms*—Brillouin optical correlation-domain reflectometry, distributed sensing, low coherence, pseudo-random modulation, strain sensing, temperature sensing.**

I. Introduction

DISTRIBUTED optical fiber sensors using Brillouin scattering have been extensively studied as key technologies in smart structures and materials [1], [2]. These sensors utilize Brillouin frequency shift (BFS) changes dependent on strain and temperature to interpret distributed strain and temperature information. Among various spatial resolution principles—time-domain [3], [4], [5], [6], frequency-domain [7], [8], and correlation-domain [9], [10], [11], [12], [13], [14], [15], [16], [17] —the focus in this context is on correlation-domain methods, which are known for their relatively high spatial resolution and unique random-access capability.

Brillouin-based correlation-domain methods can be divided into two: Brillouin optical correlation-domain analysis (BOCDA) [9], [10], [11], [12] and Brillouin optical correlation-domain reflectometry (BOCDR) [9], [13], [14], [15], [16], [17], [18], [19]. BOCDA, utilizing stimulated Brillouin scattering (SBS) in a two-end injection system, achieves a high signal-to-noise ratio (SNR) and rapid operation due to the strong signal power of SBS and lock-in detection. However, its reliance on electro-optic modulators, including a single-sideband modulator and an intensity modulator, and a lock-in amplifier leads to higher cost and system complexity. In contrast, BOCDR, employing spontaneous Brillouin scattering, operates with a lower SNR than that of BOCDA but can continue measurements up to a breakage point in the fiber under test (FUT) owing to its one-end light injection configuration.

In a standard configuration of BOCDR [13], [14], a sinusoidal-modulated laser is used as the light source. Due to the periodic nature of the sinusoidal wave, multiple correlation peaks (measurement points) are formed periodically along the FUT. Typically, the measurement range is limited to include just one correlation peak within the FUT. By controlling the modulation frequency, the correlation peak is swept along the FUT to facilitate distributed measurements. However, a significant challenge is the trade-off between measurement range and spatial resolution. Although special schemes such as temporal gating [17], double modulation [18], and chirp modulation [19] have been proposed to mitigate this issue, they have not completely eliminated the fundamental trade-off.

To address the trade-off issue in standard BOCDR, low-coherence BOCDR (LC-BOCDR) [20], [21], [22] was proposed, utilizing a low-coherence light source. A randomly modulated laser has been used in LC-BOCDR systems, but note that in LC-BOCDA, in addition to randomly modulated lasers [23],

Manuscript received 14 February 2024; revised 7 July 2024; accepted 28 July 2024. Date of publication 2 August 2024; date of current version 16 September 2024. This work was supported by JSPS KAKENHI under Grant 21H04555 and Grant 23KJ0358. *(Corresponding author: Yosuke Mizuno.)*

Kenta Otsubo, Guangtao Zhu, and Takaki Kiyozumi are with the Faculty of Engineering, Yokohama National University, Yokohama 240-8501, Japan (e-mail: otsubo-kenta-wv@ynu.jp; zhu-guangtao-jm@ynu.jp; kiyozumi-takaki-px@ynu.jp).

Kohei Noda is with the Graduate School of Engineering, University of Tokyo, Tokyo 153-8904, Japan (e-mail: knoda@cntp.t.u-tokyo.ac.jp).

Hiroshi Takahashi and Yusuke Koshikiya are with the Access Network Service Systems Laboratories, NTT Corporation, Ibaraki 305-0805, Japan (e-mail: hrsh.takahashi@ntt.com; yusuke.koshikiya@ntt.com).

Yosuke Mizuno is with the Faculty of Engineering, Yokohama National University, Yokohama 240-8501, Japan, and also with the Institute for Multidisciplinary Sciences, Yokohama National University, Yokohama 240-8501, Japan (e-mail: mizuno-yosuke-rg@ynu.ac.jp).

Color versions of one or more figures in this article are available at https://doi.org/10.1109/JLT.2024.3436928.

Digital Object Identifier 10.1109/JLT.2024.3436928

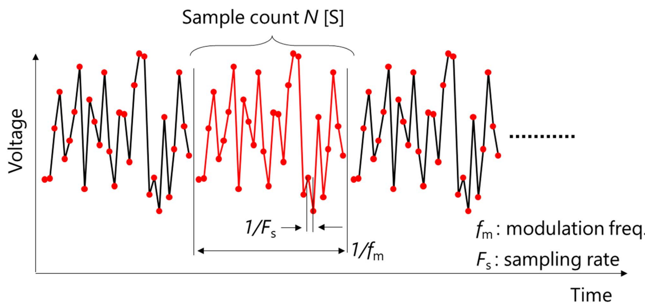

Fig. 1. Voltage waveform used for periodic pseudo-random modulation.

sources including amplified spontaneous emission (ASE) [24], [25] and chaotic lasers [26], [27] have also been employed. These light sources enable high spatial resolution determined by their coherence length, effectively addressing the direct trade-off between spatial resolution and measurement range. However, a correlation peak occurs only at the isochronous point, necessitating a variable delay line for sweeping the correlation peak along the FUT, which limits the measurement range. Pseudo-random binary sequence (PRBS) modulation in LC-BOCDA has been reported to overcome measurement range limitations [28], [29], but it still requires two-end light injection into the FUT.

In this work, we propose and demonstrate the basic operation of an LC-BOCDR system with periodic pseudo-random modulation, which operates without a variable delay line and uses single-end light injection. First, we investigate the dependence of the light source's output spectrum on modulation parameters using a delayed self-homodyne method, showcasing its potential to mitigate the trade-off between spatial resolution and measurement range. Subsequently, we demonstrate the ability to measure strain distribution along FUTs under various conditions without the need for a variable delay line. Finally, simulations indicate that this method can achieve more accurate strain distribution measurements than the standard configuration.

II. Principle

In our proposed LC-BOCDR configuration, periodic pseudo-random modulation created by an arbitrary waveform generator (AWG) is directly applied to the driving current of the light source, leading to the modulation of its output frequency. Unlike conventional LC-BOCDR based on non-periodic random modulation, this method generates multiple correlation peaks (measurement points) along the FUT, allowing sweeping of correlation peaks other than the zeroth order along the FUT without the need for a variable delay line.

The waveform used in the periodic pseudo-random modulation is shown in Fig. 1. The operation starts by generating a sequence of random voltages following a Gaussian distribution. We set a voltage range and a sample count N [S], representing the number of samples in the sequence; the unit "S" stands for "samples". This sequence is then repeatedly output at a specified sampling rate F_S [S/s] (see Fig. 1). The modulation frequency f_m, defined as the repetition rate of the single-period sequence, is given by:

$$f_m = \frac{F_S}{N}. \tag{1}$$

Similar to sinusoidal modulation, the beat signal of the light modulated with periodic signals creates correlation peaks at equal intervals centered around the isochronous point. The interval between peaks, d_m, is given by:

$$d_m = \frac{c}{2\,n\,f_m} = \frac{c\,N}{2\,n\,F_S}, \tag{2}$$

where c is the speed of light in vacuum, and n is the group index of the FUT core. By controlling F_S, the interval of correlation peaks is sequentially varied, sweeping a specific single peak along the FUT.

The spatial resolution of LC-BOCDR based on periodic pseudo-random modulation is expected to follow the same formulation as conventional non-periodically modulated LC-BOCDR. Existing LC-BOCDR systems use a laser modulated with a random sequence. As the modulation amplitude increases, the spectrum broadens and approaches a Gaussian shape, reducing the coherence of the output light. The spectra of both the reference light and Stokes light also approach Gaussian forms. The Stokes light returning from the isochronous point in the FUT interferes with the reference light, generating a zeroth-order correlation peak. While ideally, the cross-correlation of these two lights should be calculated, with sufficient modulation amplitude, their coherence lengths converge. Hence, we use the self-correlation-represented coherence function instead. When the spectral density of the light source is given by:

$$S\,(\nu) = \frac{2\sqrt{\frac{\ln 2}{\pi}}}{\Delta\nu}\,\exp\left[-4\ln 2\left(\frac{\nu-\nu_0}{\Delta\nu}\right)^2\right], \tag{3}$$

the normalized coherence function $r(\tau)$ can be determined from the Wiener-Khinchin theorem as:

$$r\,(\tau) = \exp\left[-\frac{\pi^2}{4\ln 2}\cdot(\Delta\nu\tau)^2\right]\exp\left(-j2\pi\nu_0\tau\right), \tag{4}$$

where ν_0 and $\Delta\nu$are the central frequency and occupied bandwidth of the modulated light source. The coherence time τ_c, defined as the time when $r(\tau)$ decays to 1/2, is given by [30], [31]:

$$\tau_c = \frac{2\ln 2}{\pi}\cdot\frac{1}{\Delta\nu}. \tag{5}$$

This means that only Stokes light within $\pm\tau_c$ time difference interferes with the reference light. Converting this to a distance on the FUT gives the spatial resolution. The distance Δz between two points on the FUT and the time difference τ for Stokes light to reach from these points are related by:

$$\Delta z = \frac{c\,\tau}{2\,n}. \tag{6}$$

Thus, from (5) and (6), the spatial resolution is given by:

$$\Delta z = \frac{c\,2\ln 2}{\pi\,n\,\Delta\nu}. \tag{7}$$

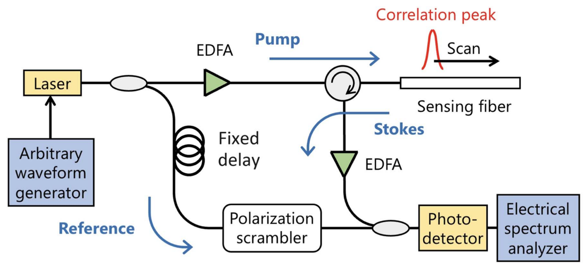

Fig. 2. Experimental setup of LC-BOCDR based on periodic pseudo-random modulation. EDFA: erbium-doped fiber amplifier.

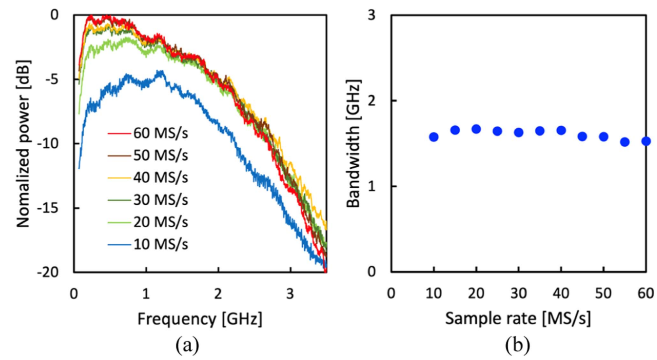

Fig. 3. Sampling rate dependencies on (a) power spectrum and (b) frequency bandwidth.

III. Experiments

A. Experimental Setup

The experimental setup for the LC-BOCDR based on periodic pseudo-random modulation is shown in Fig. 2. Its basic configuration mirrors that of a standard BOCDR setup. A distributed-feedback laser at 1550 nm was directly modulated using an AWG (SG-4222, IWATSU). The output light at 10 dBm was split into signal and reference paths via a coupler. The signal light was amplified to about 25 dBm using an erbium-doped fiber amplifier (EDFA, LXI2000, Luxpert), then injected into the FUT and the returning Stokes light was further amplified to approximately 3 dBm with another EDFA (ErFA1215, FITEL). The reference light, its polarization state averaged by a polarization scrambler (PCD104, General Photonics), was then combined with the Stokes light through a coupler. A fixed delay line with a length of 500 m was inserted in the reference path to utilize a non-zeroth-order correlation peak (the 1st-order peak was used in the demonstrations below). The heterodyne signal was converted into an electrical signal by a photodetector (PD, PR-12-B-M, Optilab) and observed with an electrical spectrum analyzer (R3273, Advantest) as the BGS. Averaging was performed 30 times on the ESA, and the sampling rate of the BFS of each sensing position was approximately 1.0 Hz, currently restricted by the switching speed of the AWG controlled using a general-purpose interface bus (GPIB).

B. Spectral Measurement

We investigated the dependence of the light source spectrum modulated by periodic pseudo-random modulation on the sampling rate. Changes in the spectral shape when varying the sampling rate were observed using a delayed self-homodyne method [32]. The modulation conditions were set to an offset of 7.0 V, a peak-to-peak amplitude of 6.0 $V_{p\text{-}p}$, and a sample count of 1000 S, with a sampling rate varied from 10 to 60 MS/s in 5 MS/s increments. The output light from the source was injected into a Mach-Zehnder interferometer, with one path including a 10 km delay fiber to provide significant time delay. The frequency resolution was about 10 kHz. The combined signals were detected with a PD and observed with an ESA (resolution bandwidth = 1 MHz, video bandwidth = 3 kHz). Gaussian fitting was performed on the obtained spectra to determine the frequency bandwidth. A portion of the observed homodyne spectrum is shown in Fig. 3(a). The spectrum overall increased up to 20 MS/s but beyond that, only the central components were strengthened. This is probably due to the laser's response not keeping up with the abrupt voltage changes in parts of the pseudo-random sequence, resulting in a reduced frequency dispersion. The bandwidth, shown in Fig. 3(b), remained relatively constant despite changes in the spectrum with the sampling rate, with a standard deviation of approximately 50 MHz. This result indicates that the sampling rate, a variable that determines the measurement range, does not affect the spatial resolution, thus not leading to the trade-off issue typically encountered in standard sinusoidal-modulation-based BOCDR.

C. Distributed Stain Measurements

To demonstrate the proof-of-concept operation of our system, we performed distributed strain measurements on FUTs under different conditions. The $\Delta\nu$ value was set to 1.65 GHz, resulting in the theoretical spatial resolution of 5.5 cm according to (7). Initially, we performed a relatively short-range measurement using a dispersion-shifted fiber (DSF) with a BFS of approximately 10.5 GHz. The structure of the FUT is shown in Fig. 4, consisting of a 140 cm DSF sandwiched between 16 m and 2 m standard silica single-mode fibers (SMFs) through fusion splicing. The 16 m silica SMF segment was a combination of 15 m and 1 m SMFs, connected using an angled-physical-contact (APC) connector, with slightly different BFS values. In addition, the 2 m SMF section was constructed from two 1 m SMFs, also connected using an APC connector, with slightly varied BFS values. Near the distal open end, a bending loss was strategically applied. The different BFS of each fiber section allowed us to treat the DSF segment as a pseudo-strain region. We varied the sampling rate from 57.20 to 58.62 MS/s with a sample count of 290 S, sweeping the 1st-order correlation peaks over 12 m around the strain region to acquire the BFS distribution. The theoretical measurement range was approximately 493 m. The results are shown in Fig. 5(a) and (b). Fig. 5(a) shows the BFS distribution along the entire measurement length, while Fig. 5(b) focuses on the 2.8 m surrounding the strain region. A steep BFS decrease of about 360 MHz was observed over approximately 140 cm, corresponding to the DSF length, which indicates successful detection of the pseudo-strain. Note that, in Fig. 5(a), abrupt BFS changes of about 40 MHz were observed around 15.0 and

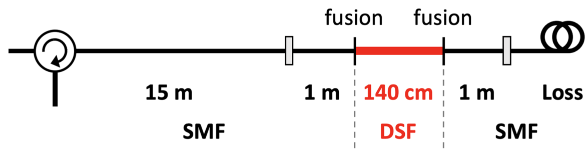

Fig. 4. Structure of the FUT used in the measurement with a shorter range. DSF: dispersion-shifted fiber, SMF: single-mode fiber.

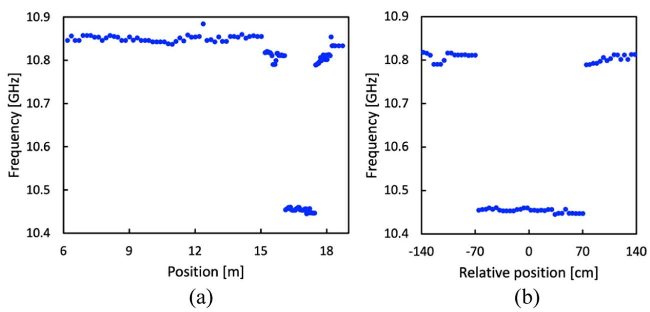

Fig. 5. Measured BFS distributions (a) along a ∼12 m fiber section and (b) around a 140 cm DSF section.

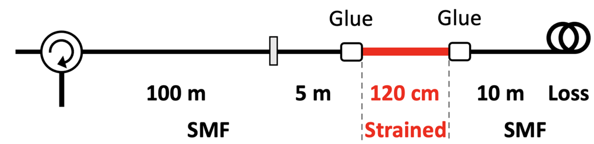

Fig. 6. Structure of the FUT used in the measurement with a longer range.

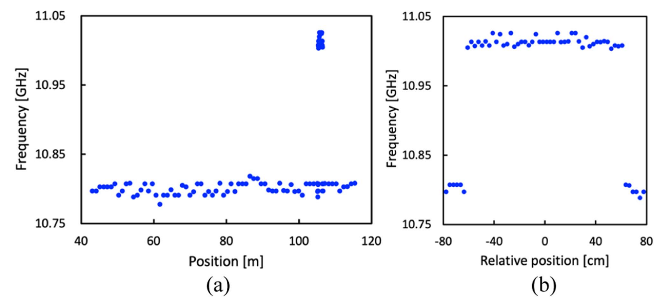

Fig. 7. Measured BFS distributions (a) along a ∼72 m fiber section and (b) around a 120 cm strained section.

18.4 m, which are attributed to the use of different types of SMFs.

Subsequently, we extended the measurement range and conducted distributed strain measurement on an FUT exceeding 100 m in length. The structure of the FUT is illustrated in Fig. 6, where approximately 0.5% strain was applied to a 120 cm section near the SMF tip. With a sample count of 320 S and a sampling rate varying from 57.0 to 60.0 MS/s, a correlation peak was swept over 72 m around the strain region to acquire the BFS distribution. The theoretical measurement range was approximately 544 m. The results are displayed in Fig. 7(a) and (b). Fig. 7(a) shows the BFS distribution for the entire measurement length, and Fig. 7(b) focuses on the 160 cm surrounding the strain region. The measured BFS change at the strained section, calculated from the averaged BFS values in the strained and non-strained sections, was approximately 220 MHz, corresponding to the BFS dependence on strain of 440 MHz/%, which closely aligns with a typical value. The high symmetry in the BFS distribution around the strained section suggests minimal systematic measurement error caused by the phase delay between amplitude modulation (AM) and frequency modulation (FM) in the laser [33], [34], [35].

As a final demonstration, we conducted a 100-m-range distributed strain measurement with a much shorter strained section. In this experiment, the delay line length was set to 10 km, utilizing the 4th-order correlation peak. The structure of the FUT is shown in Fig. 8, where approximately 0.4% strain was applied to a 10 cm section near the SMF tip. The FUT included two segments of 47 m SMFs tightly wound on mandrels, which exhibited higher BFSs compared to the loose sections. The $\Delta\nu$ value was set to 1.85 GHz, resulting in a theoretical spatial resolution of 4.8 cm. With a sample count of 290 S and a sampling rate varying from 89.3 to 91.1 MS/s, a correlation peak was swept over 100 m range, including the strained section, to acquire the BFS distribution. The theoretical measurement range was approximately 325 m. Fig. 9(a) shows the measured BFS distribution over the 100 m range. The SMF sections tightly wound on mandrels were clearly detected, exhibiting a BFS of approximately 10.96 GHz. The fluctuation in BFS is relatively large, which is expected due to the nonuniform strain applied to the SMFs wound on mandrels. At a relative position of approximately 98.5 m, the BFS change at the 10 cm strained section was also distinctly observed. The magnified view around the 10 cm strain is shown in Fig. 9(b). The BFS change amounted to approximately 180 MHz, which moderately agrees with the applied strain of 0.4%. The ratio of the measured range (∼100 m) to the detected strain length (10 cm) is approximately 1000, surpassing the theoretically maximal value for the standard configuration (∼540), which is the ratio of the theoretical measurement range to the theoretical spatial resolution. This clearly demonstrates the advantage of the periodic pseudo-random modulation configuration. It is noteworthy that the ratio of the theoretical measurement range (∼325 m) to the theoretical spatial resolution (∼4.8 cm) in this demonstration exceeds 6700.

IV. Simulation

Conventional randomly modulated LC-BOCDR is known not to produce measurement errors due to AM-FM phase delay [20]. However, whether periodic pseudo-random modulation is affected by AM-FM phase delay was a question we aimed to investigate. Following the method described in Ref. [35], we simulated the strain distribution measurements of our system. We distinguish between "intrinsic BGS," representing the BGS at each position along the FUT, and "measured BGS," the BGS as observed by BOCDR. These two BGS distributions fundamentally differ, with the measured BGS distribution derived from the square of the two-dimensional convolution of the beat spectrum and intrinsic BGS distribution. The beat spectrum is defined as the power spectrum obtained from the Fourier transform of the cross-correlation between reference and signal lights.

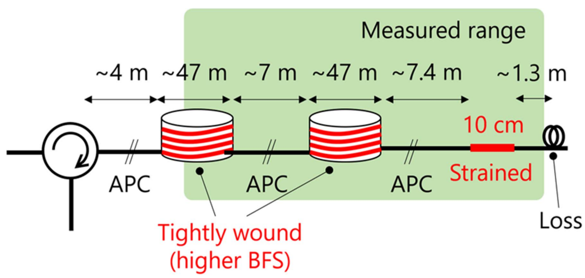

Fig. 8. Structure of the FUT used in the measurement with a longer range and a shorter strain.

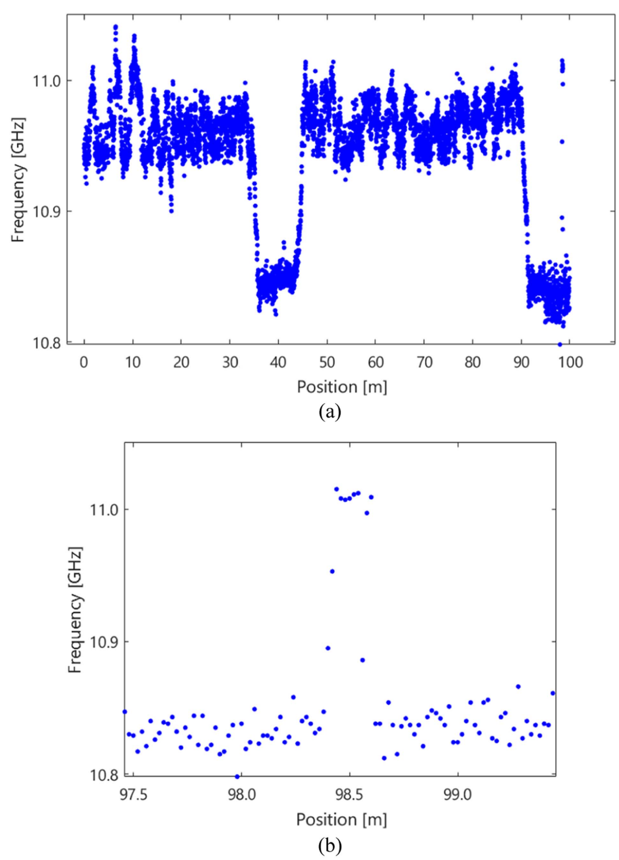

Fig. 9. Measured BFS distributions (a) along a ∼100 m fiber section and (b) around a 10 cm strained section.

For standard sinusoidal-modulation-based BOCDR, the typical beat spectrum is shown in Fig. 10(a). The modulation conditions were: frequency modulation amplitude = 4 GHz, modulation frequency = ∼1 MHz, intensity modulation power ratio = 3 dB, AM-FM phase delay = $\pi/4$, spatial resolution = ∼0.24 m. The measurement conditions were: measurement range = ∼100 m, FUT length = 5 m. The beat spectrum showed a sharp peak at relative position = 0 m, with an inverse sine distribution at other positions. The presence of AM-FM phase delay causes asymmetry in the beat spectrum. In contrast, for periodic pseudo-random-modulation-based LC-BOCDR, a typical beat spectrum is illustrated in Fig. 10(b). The measurement conditions were: sample count = 300 S, sampling rate = 60 MS/s, measurement range = ∼500 m, assuming a Gaussian random sequence with a bandwidth of 1.65 GHz. The beat

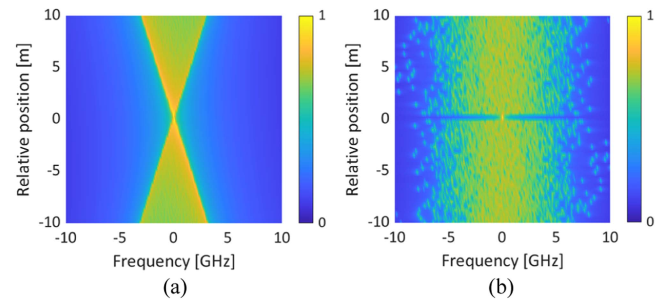

Fig. 10. Comparative beat spectra for (a) standard BOCDR with sinusoidal modulation and (b) LC-BOCDR with periodic pseudo-random modulation. The color bars show the normalized powers.

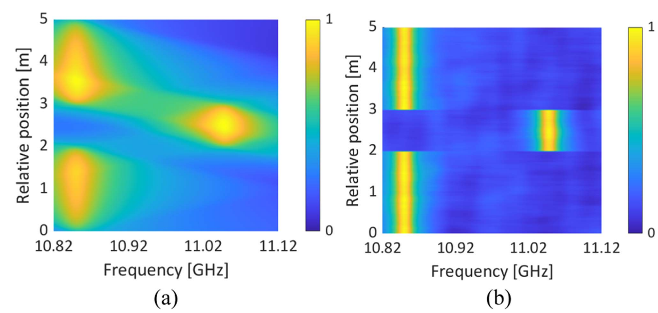

Fig. 11. Comparative "measured BGS" distributions for (a) standard BOCDR with sinusoidal modulation and (b) LC- BOCDR with periodic pseudo-random modulation. The color bars show the normalized powers.

spectrum showed a sharp peak at relative position = 0 m, with a Gaussian-like distribution at other positions. Even with AM-FM phase delay, the beat spectrum remained symmetric.

Finally, by calculating the two-dimensional convolutions of the beat spectra and intrinsic BGS distributions for both methods, we obtained the measured BGS and BFS distributions. The conditions for the intrinsic BGS distributions were: strain region = 1 m, strain magnitude = 0.4%. The comparisons of measured BGS distributions and BFS distributions for both methods are shown in Figs. 11(a), (b) and 12, respectively. The BFS distribution measured by LC-BOCDR closely resembled the actual strain distribution, indicating accurate results. These findings suggest that periodic pseudo-random-modulation-based LC-BOCDR can also reduce systematic measurement errors caused by AM-FM phase delay.

V. Conclusion

This study introduced a new approach in LC-BOCDR by employing periodic pseudo-random modulation, overcoming the conventional trade-off between spatial resolution and measurement range. Through experiments, we showed the feasibility of this method for distributed strain measurements along FUTs, with the advantage of not requiring a variable delay line. The delayed self-homodyne method revealed the modulation parameters' impact on the output spectrum of the light source, validating the potential to maintain the spatial resolution while extending the measurement range. The simulation results confirmed that this approach yields more accurate strain measurements compared to standard BOCDR, free from systematic errors

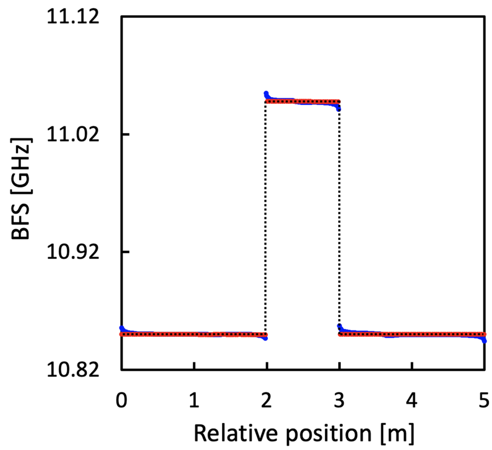

Fig. 12. BFS distributions for standard BOCDR (represented in blue) and periodic pseudo-random-modulation-based LC-BOCDR (represented in red). The black dotted lines indicate the intrinsic strain distribution, which closely aligns with the red plots.

associated with the AM-FM phase delay. This proof-of-concept sets the stage for future explorations into system optimization and in-depth performance analysis, such as enhanced spatial resolution, extended measurement range, increased measurement speed, and improved accuracy, vital areas for subsequent investigation.

References

[1] G. P. Agrawal, *Nonlinear Fiber Optics*. Boston, MA, USA: Academic, 1995.

[2] A. H. Hartog, *An Introduction to Distributed Optical Fibre Sensors*. Boca Raton, FL, USA: CRC Press, 2017.

[3] T. Horiguchi and M. Tateda, "BOTDA-nondestructive measurement of single-mode optical fiber attenuation characteristics using Brillouin interaction: Theory," *J. Lightw. Technol.*, vol. 7, no. 8, pp. 1170–1176, Aug. 1989, doi: 10.1109/50.32378.

[4] T. Kurashima, T. Horiguchi, H. Izumita, S. Furukawa, and Y. Koyamada, "Brillouin optical-fiber time domain reflectometry," *IEICE Trans. Commun.*, vol. E76-B, no. 4, pp. 382–390, 1993.

[5] M. A. Soto, Z. Yang, J. A. Ramírez, S. Zaslawski, and L. Thévenaz, "Evaluating measurement uncertainty in Brillouin distributed optical fibre sensors using image denoising," *Nature Commun.*, vol. 12, Aug. 2021, Art. no. 4901, doi: 10.1038/s41467-021-25114-4.

[6] Y. Wang, L. Chen, and X. Bao, "Single-shot chirped pulse BOTDA for static and dynamic strain sensing," *Opt. Lett.*, vol. 46, no. 22, pp. 5774–5777, 2021, doi: 10.1364/OL.441815.

[7] D. Garus, K. Krebber, F. Schliep, and T. Gogolla, "Distributed sensing technique based on Brillouin optical-fiber frequency-domain analysis," *Opt. Lett.*, vol. 21, no. 17, pp. 1402–1404, Sep. 1996, doi: 10.1364/OL.21.001402.

[8] A. Minardo, R. Bernini, R. Ruiz-Lombera, J. Mirapeix, J. M. Lopez-Higuera, and L. Zeni, "Proposal of Brillouin optical frequency-domain reflectometry (BOFDR)," *Opt. Exp.*, vol. 24, no. 26, pp. 29994–30001, Dec. 2016, doi: 10.1364/OE.24.029994.

[9] K. Hotate, "Brillouin optical correlation-domain technologies based on synthesis of optical coherence function as fiber optic nerve systems for structural health monitoring," *Appl. Sci.*, vol. 9, no. 1, Jan. 2019, Art. no. 187, doi: 10.3390/app9010187.

[10] K. Hotate and T. Hasegawa, "Measurement of Brillouin gain spectrum distribution along an optical fiber using a correlation-based technique–proposal experiment and simulation," *IEICE Trans. Electron.*, vol. E83-C, no. 3, pp. 405–412, Mar. 2000.

[11] B. Wang, X. Fan, Y. Fu, and Z. He, "Dynamic strain measurements based on high-speed single-end-access Brillouin optical correlation domain analysis," *J. Lightw. Technol.*, vol. 37, no. 11, pp. 2557–2567, Jun. 2019, doi: 10.1109/JLT.2018.2883386.

[12] Z. Li, Y. Zhou, B. Jiang, X. Gan, L. Yan, and J. Zhao, "Dynamic strain measurement based on ultrafast Brillouin collision in the correlation domain," *Opt. Lett.*, vol. 46, no. 14, pp. 3488–3491, 2021, doi: 10.1364/OL.426181.

[13] Y. Mizuno, W. Zou, Z. He, and K. Hotate, "Proposal of Brillouin optical correlation-domain reflectometry (BOCDR)," *Opt. Exp.*, vol. 16, no. 16, pp. 12148–12153, Jul. 2008, doi: 10.1364/OE.16.012148.

[14] Y. Mizuno, W. Zou, Z. He, and K. Hotate, "Operation of Brillouin optical correlation-domain reflectometry: Theoretical analysis and experimental validation," *J. Lightw. Technol.*, vol. 28, no. 22, pp. 3300–3306, Nov. 2010, doi: 10.1109/JLT.2010.2081348.

[15] Y. Mizuno, N. Hayashi, H. Fukuda, K. Y. Song, and K. Nakamura, "Ultrahigh-speed distributed Brillouin reflectometry," *Light Sci. Appl.*, vol. 5, Jun. 2016, Art. no. e16184, doi: 10.1038/lsa.2016.184.

[16] G. Zhu, K. Kishizawa, K. Noda, H. Lee, K. Nakamura, and Y. Mizuno, "Wide-dynamic-range Brillouin optical correlation-domain reflectometry with 20-kHz sampling rate," *IEEE Sensors J.*, vol. 22, no. 7, pp. 6644–6650, Apr. 2022, doi: 10.1109/JSEN.2022.3153169.

[17] Y. Mizuno, Z. He, and K. Hotate, "Measurement range enlargement in Brillouin optical correlation-domain reflectometry based on temporal gating scheme," *Opt. Exp.*, vol. 17, no. 11, pp. 9040–9046, May 2009, doi: 10.1364/OE.17.009040.

[18] Y. Mizuno, Z. He, and K. Hotate, "Measurement range enlargement in Brillouin optical correlation-domain reflectometry based on double-modulation scheme," *Opt. Exp.*, vol. 18, no. 6, pp. 5926–5933, 2010, doi: 10.1364/OE.18.005926.

[19] K. Noda, H. Lee, K. Nakamura, and Y. Mizuno, "Measurement range enlargement in Brillouin optical correlation-domain reflectometry based on chirp modulation scheme," *Appl. Phys. Exp.*, vol. 13, no. 8, Jul. 2020, Art. no. 082003, doi: 10.35848/1882-0786/aba151.

[20] K. Otsubo et al., "Systematic-error suppression in low-coherence Brillouin optical correlation-domain reflectometry," *Sci. Rep.*, vol. 13, Oct. 2023, Art. no. 17531, doi: 10.1038/s41598-023-44801-4.

[21] K. Otsubo, T. Kiyozumi, K. Noda, K. Nakamura, H. Lee, and Y. Mizuno, "High-resolution low-coherence Brillouin optical correlation-domain reflectometry with suppressed systematic error," presented at the 28th Int. Conf. Opt. Fiber Sensors, Hamamatsu-shi, Japan, Nov. 20–24, 2023, Paper W4.46, doi: 10.1364/OFS.2023.W4.46.

[22] M. Zhang et al., "Impact of Brillouin amplification on the spatial resolution of noise-correlated Brillouin optical reflectometry," *Chin. Opt. Lett.*, vol. 15, no. 8, 2017, Art. no. 080603, doi: 10.3788/COL201715.080603.

[23] K. Hotate, W. Goh, Y. Mizuno, and Z. He, "Brillouin optical correlation-domain analysis based on simultaneous utilization of sinusoidal and noise modulation," *Proc. IEICE Gen. Conf.*, vol. 2008, 2008, Art. no. 469.

[24] R. Cohen, Y. London, Y. Antman, and A. Zadok, "Brillouin optical correlation domain analysis with 4 millimeter resolution based on amplified spontaneous emission," *Opt. Exp.*, vol. 22, no. 10, pp. 12070–12078, 2014, doi: 10.1364/OE.22.012070.

[25] A. Zarifi et al., "Highly localized distributed brillouin scattering response in a photonic integrated circuit," *APL Photon.*, vol. 3, no. 3, Mar. 2018, Art. no. 036101, doi: 10.1063/1.5000108.

[26] J. Zhang, C. Feng, M. Zhang, Y. Liu, C. Wu, and Y. Wang, "Brillouin optical correlation domain analysis based on chaotic laser with suppressed time delay signature," *Opt. Exp.*, vol. 26, no. 6, pp. 6962–6972, 2018, doi: 10.1364/OE.26.006962.

[27] Y. Wang et al., "Millimeter-level-spatial-resolution Brillouin optical correlation-domain analysis based on broadband chaotic laser," *J. Lightw. Technol.*, vol. 37, no. 15, pp. 3706–3712, Aug. 2019, doi: 10.1109/JLT.2019.2916801.

[28] A. Zadok, Y. Antman, N. Primerov, A. Deniso, J. Sancho, and L. Thevenaz, "Random-access distributed fiber sensing," *Laser Photon. Rev.*, vol. 6, no. 5, pp. L1–L5, Sep. 2012, doi: 10.1002/lpor.201200013.

[29] Y. London, Y. Antman, E. Preter, N. Levanon, and A. Zadok, "Brillouin optical correlation domain analysis addressing 440,000 resolution points," *J. Lightw. Technol.*, vol. 34, no. 19, pp. 4421–4429, Oct. 2016, doi: 10.1109/JLT.2016.2521173.

[30] A. F. Fercher, "Optical coherence tomography," *J. Biomed. Opt.*, vol. 1, pp. 157–173, Apr. 1996, doi: 10.1117/12.231361.

[31] J. M. Schmitt, "Optical coherence tomography (OCT): A review," *IEEE J. Sel. Topics Quantum Electron.*, vol. 5, no. 4, pp. 1205–1215, Jul./Aug. 1999, doi: 10.1109/2944.796348.

[32] T. Okoshi, K. Kikuchi, and A. Nakayama, "Novel method for high resolution measurement of laser output spectrum," *Electron. Lett.*, vol. 16, no. 16, pp. 630–631, Jul. 1980, doi: 10.1049/el:19800437.

[33] K. Y. Song and J. H. Choi, "Measurement error induced by the power-frequency delay of the light source in optical correlation-domain distributed Brillouin sensors," *Opt. Lett.*, vol. 43, no. 20, pp. 5078–5081, Oct. 2018, doi: 10.1364/OL.43.005078.

[34] K. Y. Song, J. H. Youn, and J. H. Choi, "Suppression of systematic errors in Brillouin optical correlation domain analysis based on injection-locking," *J. Lightw. Technol.*, vol. 37, no. 17, pp. 4421–4425, Sep. 2019, doi: 10.1109/JLT.2019.2925252.

[35] G. Zhu, K. Noda, H. Lee, K. Nakamura, and Y. Mizuno, "Error compensation in Brillouin optical correlation-domain reflectometry by combining bidirectionally measured frequency shift distributions," *Appl. Phys. Exp.*, vol. 14, no. 5, May 2021, Art. no. 052006, doi: 10.35848/1882-0786/abfb40.

Kenta Otsubo received the B.E. degree in electrical and computer engineering in 2022 from Yokohama National University, Japan, where he has been working toward the M.E. degree in electrical and computer engineering focusing on distributed fiber-optic sensing techniques, with a particular interest in low-coherence Brillouin optical correlation-domain reflectometry since 2020.

He was the recipient of the Outstanding Student Award 2023 from the Optical Fiber Technologies Conference (OFT), Institute of Electronics, Information and Communication Engineers (IEICE) of Japan. He is also a Student Member of the Japanese Society of Applied Physics (JSAP).

Guangtao Zhu received the B.E. degree in light source and lighting from the Taiyuan University of Technology, Taiyuan, China, in 2020, and the M.E. degree in electrical and computer engineering in 2023 from Yokohama National University, Yokohama, Japan, where he is currently working toward the Dr.Eng. degree in distributed fiber-optic Brillouin sensing. He was recipient of the President's Award from Yokohama National University in 2022. He is also a Student Member of the Japanese Society of Applied Physics (JSAP).

Kohei Noda (Member, IEEE) received the B.E., M.E., and Dr. Eng. degrees in electrical and electronic engineering from the Tokyo Institute of Technology, Tokyo, Japan, in 2018, 2020, and 2023, respectively, focusing on the distributed fiber-optic polarization sensing.

Since 2023, he has been with the University of Tokyo, as a Research Fellow (PD) of the Japan Society for the Promotion of Science (JSPS). His research focuses on advanced fiber-optic sensing.

Dr. Noda was the recipient of the Outstanding Student Poster Award 2019 from the Optical Fiber Technologies Conference (OFT), Institute of Electronics, Information and Communication Engineers (IEICE) of Japan, the Optical Society of America (OSA) Student Prize from the 8th Asia-Pacific Optical Sensors Conference (APOS) in 2019, and Outstanding Student Award 2020, OFT, IEICE. He is also a Member of the Japanese Society of Applied Physics (JSAP).

Takaki Kiyozumi (Student Member, IEEE) received the B.E. degree in electrical and computer engineering in 2022 from Yokohama National University, Yokohama, Japan, where he has been working toward the M.E. degree in electrical and computer engineering focusing on distributed fiber-optic sensing techniques since 2020.

He was the recipient of the IEEE IM Japan Chapter Student Award 2021, Outstanding Student Award 2021 from the Optical Fiber Technologies Conference (OFT), Institute of Electronics, Information and Communication Engineers (IEICE) of Japan, and the Best Student Paper Award from the 27th Optoelectronics and Communications Conference (OECC 2022). He is also a Student Member of the IEEE and the Japanese Society of Applied Physics (JSAP).

Hiroshi Takahashi received the B.E. degree in electrical engineering from the Tokyo University of Science, Tokyo, Japan, in 2008, and the M.E. degree in electrical engineering and information systems from the University of Tokyo, Tokyo, in 2010.

In 2010, he joined the Access Network Service Systems Laboratories, NTT Corporation, Japan, where he has been engaged in research on optical measurement and maintenance technologies for optical fiber networks.

He is also a Member of the Institute of Electronics, Information and Communication Engineers (IEICE) of Japan.

Yusuke Koshikiya received the B.E. and M.E. degrees in mechanical engineering and the Ph.D. degree in electrical engineering from Waseda University, Tokyo, Japan, in 2001, 2003, and 2015, respectively.

In 2003, he joined the Access Network Service Systems Laboratories, NTT Corporation, Japan, where he has been engaged in research on optical measurement and maintenance technologies for optical fiber networks. He is currently a Group Leader. His research interests include optical fiber sensing and optical fiber measurements.

Dr. Koshikiya was the recipient of the IEEE Laser and Electro-Optics Society Japan Chapter Young Scientist Award in 2004. He is also a Member of the Institute of Electronics, Information and Communication Engineers (IEICE) of Japan.

Yosuke Mizuno (Senior Member, IEEE) received the B.E., M.E., and Dr. Eng. degrees in electronic engineering from the University of Tokyo, Tokyo, Japan, in 2005, 2007, and 2010, respectively.

From 2010 to 2012, as a Research Fellow (PD) of the Japan Society for the Promotion of Science (JSPS), he worked on polymer optics at Tokyo Institute of Technology, Japan. In 2011, he was with the BAM Federal Institute for Materials Research and Testing, Germany, as a Visiting Research Associate. From 2012 to 2020, he was an Assistant Professor with the Tokyo Institute of Technology, Tokyo. Since 2020, he has been an Associate Professor with the Faculty of Engineering, Yokohama National University, where he is active in fiber-optic sensing and polymer optics.

Prof. Mizuno was the recipient of the Funai Information Technology Award 2017, Optics Design Award 2018, and Young Scientist's Award 2021, Commendation for Science and Technology, Minister of Education, Culture, Sports, Science and Technology (MEXT). He is also a Senior Member of the IEEE Photonics Society and a Member of the Japanese Society of Applied Physics (JSAP), Optical Society of Japan (OSJ), and Institute of Electronics, Information and Communication Engineers (IEICE) of Japan.